RSC Medicinal Chemistry

ROYAL SOCIETY OF CHEMISTRY

RESEARCH ARTICLE

View Article Online
View Journal | View Issue

Cite this: *RSC Med. Chem.*, 2026, **17**, 1099

Mitochondria-targeting symmetric diiminoguanidines: potent and selective anticancer agents against pancreatic tumors

Sigrid Lacaille* and Andreea R. Schmitzer *

Received 11th September 2025,
Accepted 19th December 2025

DOI: 10.1039/d5md00808e

rsc.li/medchem

Pancreatic cancer remains one of the deadliest malignancies of the 21st century, with a five-year survival rate below 12%. Its growing incidence is strongly linked to modern lifestyles, marked by obesity, diabetes, overnutrition, and physical inactivity. Current chemotherapies offer limited success and are often burdened by severe side effects, highlighting the urgent need for more effective and selective treatments. In response, we have developed a new class of easily synthesized, amphiphilic symmetric diiminoguanidines and evaluated their antiproliferative activity against pancreatic cancer cell lines. Several compounds demonstrated remarkable efficacy and selectivity, positioning them as strong candidates for further *in vivo* evaluation. Fluorescence microscopy revealed that these molecules rapidly localize into mitochondria. Preliminary mechanistic studies suggest their primary target is the mitochondrial respiratory chain. These findings support the potential of diiminoguanidines as affordable, mitochondria-targeting alternatives to existing pancreatic cancer therapies.

Introduction

Pancreatic cancer stands as one of the most aggressive and fatal malignancies in modern oncology.[1–3] With a dismal five-year survival rate of less than 12%, it is projected to become the second leading cause of cancer-related deaths in the United States by 2040, surpassing colorectal cancer and second only to lung cancer.[3,4] This alarming trend reflects both the increasing incidence of the disease and the lack of effective therapeutic interventions.[5,6]

The rising prevalence of pancreatic cancer in Western societies is closely tied to metabolic and lifestyle-associated risk factors. Type 2 diabetes, obesity, overnutrition, and physical inactivity have been consistently identified as key contributors to pancreatic tumorigenesis.[7–11] These conditions, highly prevalent in North America and Europe, create a metabolic and inflammatory environment that fosters cancer development and progression. One of the principal challenges in treating pancreatic cancer is the late-stage diagnosis in most patients. Early clinical signs are either vague or absent, often mistaken for benign gastrointestinal disorders. By the time a definitive diagnosis is made, the disease is frequently at an advanced or metastatic stage, leaving few curative options. Surgical resection, while potentially curative, is only feasible in a minority of cases due to the pancreas's deep retroperitoneal location, rich vascular supply, and the high metastatic potential of pancreatic tumors.[11]

Chemotherapy remains the cornerstone of treatment for unresectable or metastatic pancreatic cancer. However, current regimens offer only modest improvements in survival and are associated with significant toxicity. Antimetabolites such as 5-fluorouracil (5-FU) and capecitabine disrupt RNA and DNA synthesis but are burdened with adverse effects including myelosuppression, neurotoxicity, and gastrointestinal damage.[12–17] Combination therapies like FOLFIRINOX (5-FU, folinic acid, irinotecan, and oxaliplatin) improve efficacy but also amplify systemic toxicity, often limiting their use to patients with good performance status.[18–20] Gemcitabine, a nucleoside analog, remains the standard of care in many settings, yet typically extends survival by only a few months.[21–25] These clinical limitations underscore the urgent need for novel therapeutic strategies that are both efficacious and well-tolerated.

Mitochondria, the powerhouses of the cell, have emerged as promising targets in cancer therapy due to their essential roles in bioenergetics, apoptosis regulation, and reactive oxygen species (ROS) generation.[26–28] Compounds that selectively disrupt mitochondrial function in cancer cells could represent a powerful new avenue for treatment, particularly in metabolically active and chemoresistant cancers such as pancreatic adenocarcinoma.[29–32]

Over the past decade, our group has concentrated on the development of guanidine-based molecules, particularly

Département de chimie- Faculté des arts et des sciences, Université de Montréal. Campus MIL, 1375, Ave. Thérèse Lavoie-Roux, Montréal, Québec, H2V 0B3, Canada. E-mail: ar.schmitzer@umontreal.ca

biguanides, as promising agents for targeting pancreatic cancer cells (Fig. 1). We previously demonstrated that amphiphilic biguanide salts, most notably a triflate salt of phenylethynylbenzyl (PEB)-substituted biguanide, exhibited potent antiproliferative activity, with IC_{50} values in the low micromolar range against pancreatic cancer cell lines.[33,34] Building on these findings, we further explored bifunctional constructs, including biguanide-based PROTACs and AUTA Cs, which induced mitochondrial accumulation and led to marked growth inhibition.[35,36] These efforts validated the guanidine scaffold as a versatile and bioactive platform in anticancer drug discovery.

Encouraged by these results, we hypothesized that another class of guanidine derivatives, iminoguanidines, could serve as valuable building blocks for the design of new amphiphilic molecules with anticancer potential. Like biguanides, iminoguanidines possess basic nitrogen atoms capable of protonation and hydrogen bonding, key features for mitochondrial targeting and intracellular accumulation.[37] Moreover, their synthetic accessibility enables rapid generation of structural analogs, facilitating structure–activity relationship (SAR) exploration. In this study, we report the synthesis of a library of amphiphilic symmetric diiminoguanidines, prepared as chloride salts, bearing a range of aromatic, polycyclic aromatic, and heterocyclic substituents. These compounds were evaluated for their antiproliferative activity on pancreatic cancer cell lines. Selectivity toward cancer *versus* normal cells was assessed, and mechanistic studies were conducted to elucidate their mode of action, with a particular focus on mitochondrial targeting.

Results and discussion

Design and synthesis of amphiphilic symmetric diiminoguanidines as chloride salts

A series of 14 symmetric diiminoguanidines were synthesized as chloride salts (Fig. 2) in order to explore the relationship between molecular structure, specifically side-chain identity and antiproliferative activity against pancreatic cancer cells. Amphiphilicity was a critical design parameter, as it strongly influences a molecule's ability to traverse cell membranes and reach intracellular organelles, such as mitochondria. To modulate amphiphilicity and molecular recognition features, we introduced aromatic rings (both substituted and unsubstituted), polycyclic aromatic systems, and heterocycles as side chains. Aromatic moieties are prevalent in medicinal chemistry due to their capacity for π–π stacking interactions, while polycyclic aromatics offer advantageous photophysical properties for intracellular tracking. Heterocycles, on the other hand, are biocompatible and capable of hydrogen bonding, enhancing their potential to interact with biological targets. The diiminoguanidines were obtained *via* double condensation of *N*,*N*′-diaminoguanidinium hydrochloride with two equivalents of the corresponding aldehydes in methanol, under mild conditions (room temperature to 80 °C, ≤24 h) (Fig. 2). It should be noted that certain compounds were obtained with low yields. In the case of the polycyclic aromatic compounds, the main reason was the low solubility of the final substituted diiminoguanidine hydrochloride in methanol. In the case of the heterocyclic compounds, even higher temperatures or longer reaction times did not allow the increase of the yields.

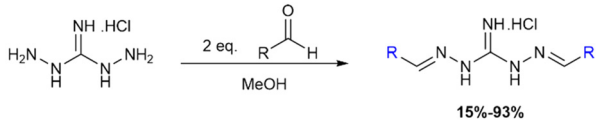

1a: R=phenyl
1b: R=*p*-fluorophenyl
1c: R=*p*-chlorophenyl
1d: R=3,5-dimethylphenyl
1e: R=3,5-bis(trifluoro)methylphenyl
2a: R=2-naphtyl
2b: R=9-phenantryl
2c: R=1-pyrenyl
3a: R=2-thiophenyl
3b: R=2-imidazole
3c: R=2-pyridinyl
3d: R=2-pyrole
3e: R=5-indole
3f: R=5-pyrimidine

Fig. 2 Structure of the synthesized symmetric diiminoguanidines.

Generally, this synthetic route is operationally simple, efficient, and adheres to green chemistry principles, an important consideration in the development of sustainable therapeutic candidates.

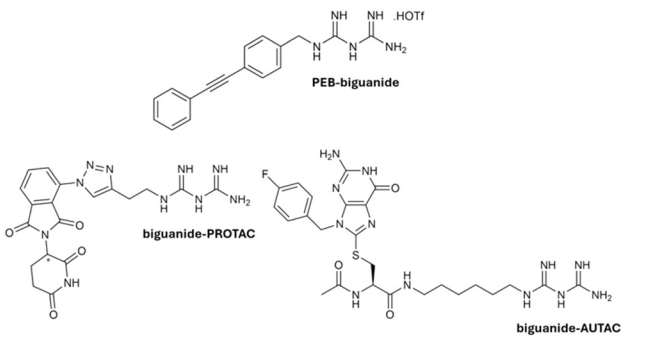

Fig. 1 Structure of antiproliferative PEB-biguanide, biguanide-PROTAC and biguanide-AUTAC synthesized in our group.

Antiproliferative activity of the diiminoguanidine hydrochlorides

The antiproliferative properties of the synthesized diiminoguanidines were evaluated on two human pancreatic cancer cell lines: KP4, which is characterized by a high metastatic potential, and PANC1, associated with a comparatively more moderate phenotype. As shown in Table 1, all compounds exhibited IC_{50} (concentration that inhibit cancer cell growth by 50%) in the micromolar range, validating the iminoguanidine scaffold as a promising starting point for the development of anticancer agents. Remarkably, compound **3b**, bearing imidazole side chains, demonstrated the most potent activity with an IC_{50} of 280 nM, while **2c**, bearing pyrene groups, was the least active (IC_{50} = 163 μM).

SAR analysis revealed several trends:

Table 1 IC_{50} values of diiminoguanidines on pancreatic cancer cell lines KP4 and PANC1, on healthy cell lines IMR90 and *hTERT*-HPNE and selectivity indexes

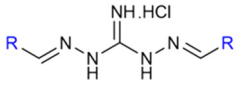

Compound	Substituent R	IC_{50} cancer cells (μM)		IC_{50} healthy cells (μM)		SI	SI	clog P^a
		KP4	PANC1	IMR90	hTERT-HPNE	IMR90/PANC1	hTERT-HPNE/PANC1	
1a	Phenyl	9.3 ± 1.4	29.6 ± 2.9	23.6 ± 0.9	62.9 ± 7.5	0.8	2.1	2.24
1b	*p*-Fluorophenyl	9.4 ± 1.3	28.6 ± 4.3	16.3 ± 2.9	50.0 ± 5.4	0.6	1.7	2.83
1c	*p*-Chlorophenyl	36.6 ± 5.5	59.1 ± 4.1	43.5 ± 5.2	48.5 ± 9.7	0.7	0.8	3.29
1d	3,5-Dimethylphenyl	29.1 ± 3.5	56.2 ± 3.4	89.1 ± 5.3	140.7 ± 21.1	3.4	6.4	3.57
1e	3,5-Bis(trifluoro)methylphenyl	134.0 ± 10.7	58.2 ± 8.4	197.0 ± 27.6	374.9 ± 30.0	1.6	2.5	6.4
2a	2-Naphtyl	122.2 ± 21.9	104.7 ± 7.3	119.2 ± 27.4	276.0 ± 55.2	1.1	2.6	4.05
2b	9-Phenantryl	138.6 ± 16.6	151.4 ± 13.6	190.5 ± 24.7	130.6 ± 10.4	1.3	0.9	5.83
2c	1-Pyrenyl	163.2 ± 24.5	240.3 ± 28.3	280.9 ± 25.3	284.3 ± 54	1.2	1.2	6.76
3a	2-Thiophenyl	10.8 ± 1.7	50.1 ± 6.0	47.9 ± 7.7	120.8 ± 20.5	1	2.4	2.26
3b	2-Imidazole	0.28 ± 0.02	9.7 ± 1.3	180.1 ± 10.8	257.9 ± 33.5	18.6	26.6	−0.63
3c	2-Pyridinyl	5.4 ± 1.0	4.8 ± 0.3	95.0 ± 4.6	198.8 ± 23.8	19.8	41.4	0.78
3d	2-Pyrole	0.52 ± 0.03	4.1 ± 0.3	21.6 ± 2.6	74.3 ± 7.4	5.3	18.1	0.62
3e	2-Indole	4.9 ± 0.4	7.01 ± 1.2	5.9 ± 1.0	8.8 ± 0.8	0.8	1.3	2.47
3f	5-Pyrimidine	118.9 ± 14.3	113.5 ± 22.7	95.6 ± 17.2	398.1 ± 55.7	0.8	3.5	−0.42

[a] Calculated with Swiss ADME consensus.

• Heterocyclic side chains (**3a–3f**) generally conferred higher potency. Imidazole- and oxazole-bearing compounds showed IC_{50} values well below 5 μM. The exception was **3f** (pyrimidine), which showed only modest activity (IC_{50} = 119 μM), suggesting that not all heterocycles contribute equally to activity.

• Polycyclic aromatic derivatives (**2a–2c**), such as those containing pyrene (**2c**) or phenanthracene (**2b**) moieties, were the least active. Their high lipophilicity may hinder cell membrane penetration or intracellular distribution.

• Phenylic derivatives (**1a–1e**) showed variable activity with no clear correlation to electronic effects. For example, the unsubstituted phenyl derivative **1a** and its *para*-fluorinated analog **1b** exhibited similar activity. Interestingly, a *meta*-substituted derivative bearing electron-donating methyl groups (**1d**) yielded an IC_{50} of 29 μM, whereas its electron-withdrawing trifluoromethylphenyl counterpart (**1e**) had a significantly reduced activity (IC_{50} = 134 μM). This observation points to a complex interplay of steric and electronic factors not solely explained by traditional SAR paradigms.

As imine bonds are known to have the ability to be hydrolyzed in acidic aqueous media, we investigated the stability of our compounds. To do so, we mimicked the biological experimental conditions, namely PBS buffer with 4% DMSO at 37 °C for 3 days, and recorded the UV-Vis spectrum every 24 hours. All the recorded spectra were identical, confirming no deterioration of the diiminoguanidine structure for the duration of treatment (see SI).

Role of amphiphilicity (clog *P*) in antiproliferative activity

To further investigate the impact of amphiphilicity on biological performance, we analyzed the correlation between the calculated log *P* (clog *P*) values and IC_{50} data (Fig. 3). The results revealed a compelling inverse relationship between amphiphilicity and antiproliferative efficacy. Compounds with clog *P* values between 0.5 and 4 consistently showed strong activity (IC_{50} < 50 μM), indicating an optimal amphiphilic window that supports both membrane permeability and intracellular distribution. In contrast, compounds with clog *P* values > 4 exhibited significantly reduced potency (IC_{50} > 100 μM), likely due to excessive lipophilicity that hinders effective cellular uptake. Compound **3f**, with a clog *P* of −0.42, displayed weak activity (IC_{50} = 119 μM), suggesting that higher hydrophilicity may also be detrimental. However, the high activity of **3b** despite its higher hydrophilicity suggests that this is not the only parameter that can explain the cytotoxicity of the studied diiminoguanidines. Overall, these results emphasize the necessity of fine-tuning amphiphilicity of the compounds to achieve an optimal balance for membrane penetration, intracellular targeting, and pharmacological activity.

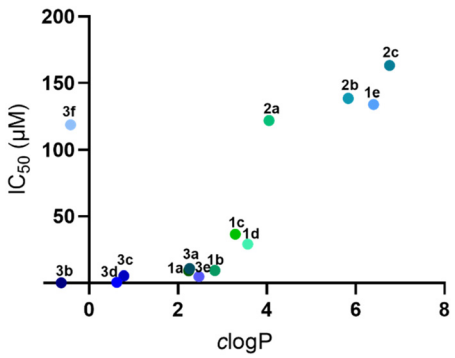

Fig. 3 Correlation between clog *P* and IC_{50} values of diiminoguanidines on KP4 pancreatic cancer cells.

Nevertheless, only a deep study of the mechanism of action and the determination of the precise target of diiminoguanidines in the cells would allow to establish the relationship between the nature of the substituents and their cytotoxic activity.

Selectivity toward cancer *versus* normal cells

To evaluate the selectivity of our diiminoguanidines for pancreatic cancer cells over non-cancerous cells, we assessed their antiproliferative activity on two healthy human cell lines: hTERT-HPNE (immortalized pancreatic epithelial cells) and IMR-90 (normal human lung fibroblasts). hTERT-HPNE serves as a physiological control representative of the targeted organ, while IMR-90 represents a non-tumorigenic, proliferative cell line that is often sensitive to chemotherapeutic toxicity, providing a stringent measure of off-target effects. Selectivity indices (SI), calculated as the ratio of IC_{50} in healthy cells to that in cancer cells, revealed important trends. Compounds bearing phenylic (**1a–1e**) and polycyclic aromatic (**2a–2c**) side chains exhibited indices low selectivity (SI < 10), suggesting a narrow therapeutic window and potential for toxicity in non-cancerous tissues. In contrast, some heterocyclic derivatives (**3a–3d**) showed higher selectivity. Notably, compounds **3b–3d**, which featured imidazole (**3b**), pyridine (**3c**), and pyrrole (**3d**) side chains, respectively, stood out as the most selective candidates. Compound **3b**, in particular, achieved a selectivity index greater than 600 for KP4 cells relative to both hTERT-HPNE and IMR-90 lines, indicating strong preferential activity against malignant cells with minimal cytotoxicity toward normal tissue. Given their potent antiproliferative activity and favorable selectivity profiles, these heterocycle-functionalized diiminoguanidines, especially **3b**, represent promising leads for further *in vivo* evaluation. Their strong discrimination between cancerous and normal cells positions them as attractive candidates for the development of targeted pancreatic cancer therapies with reduced systemic toxicity.

Selectivity indexes were calculated for PANC1 cancer cells as well, and can be found in SI. Overall, the selectivity indexes on PANC1 cancer cells were in the same range as the one for KP4, except for compound **3b**, suggesting no preference for a particular pancreatic cancer cell line.

Mechanism of action

In light of the potent antiproliferative activity demonstrated by our diiminoguanidines, we next investigated their cellular mechanism of action. Given the amphiphilic and cationic nature of these compounds, characteristics known to facilitate mitochondrial targeting, particularly among guanidinium-containing structures, we hypothesized that mitochondria might be their primary intracellular site of action. To test this, we exploited the inherent fluorescence properties of several of our diiminoguanidine derivatives and performed confocal fluorescence microscopy on live pancreatic cancer cells. Cells were co-stained with

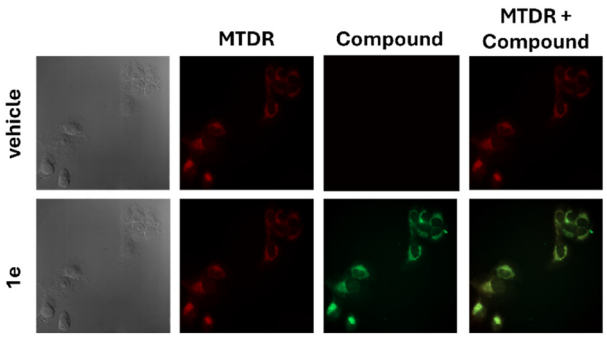

Fig. 4 Confocal microscopy images of KP4 pancreatic cancer cells treated with 100 nM diiminoguanidine hydrochloride **1e** or vehicle (4% DMSO) and colocalization with MitoTracker deep red (zoom × 63).

MitoTracker™ Deep Red (MTDR), a well-established mitochondrial marker, allowing us to assess potential colocalization. The resulting images revealed a strong spatial overlap between the fluorescent signal of our compounds and that of MTDR. This colocalization was visually confirmed by the emergence of yellow signals in merged images (Fig. 4 and SI), and quantitatively supported by Pearson correlation coefficients exceeding 0.89 for all tested compounds—indicative of a robust mitochondrial localization.

To further characterize this localization, we conducted time-course experiments to evaluate the persistence of mitochondrial targeting. Cells treated with diiminoguanidines were imaged at 30 minutes and 24 hours post-incubation. Remarkably, mitochondrial accumulation was evident as early as 30 minutes and remained clearly detectable after 24 hours, indicating that these compounds are not rapidly cleared and instead exhibit sustained mitochondrial residency. Taken together, these findings confirm that our amphiphilic symmetric diiminoguanidines rapidly and durably accumulate in mitochondria. This prolonged retention is likely critical for their antiproliferative efficacy, enabling them to engage mitochondrial targets involved in energy production or apoptosis regulation over an extended period. The observed mitochondrial tropism not only highlights a key feature of the compounds' mechanism of action but also strengthens their candidacy as selective anticancer agents.

Action on the mitochondrial respiratory chain

Mitochondrial dysfunction is a common consequence of therapeutic agents that accumulate within these organelles. When the mitochondrial respiratory chain (MRC) is impaired, cancer cells often respond by shifting their energy production toward aerobic glycolysis, a metabolic reprogramming known as the Warburg effect. To determine whether our diiminoguanidines interfere with mitochondrial respiration, we employed a glycolytic suppression assay using 2-deoxyglucose (2-DG), a well-characterized glycolysis inhibitor. 2-DG is a glucose analog in which the hydroxyl group at the 2-position is absent. This structural modification

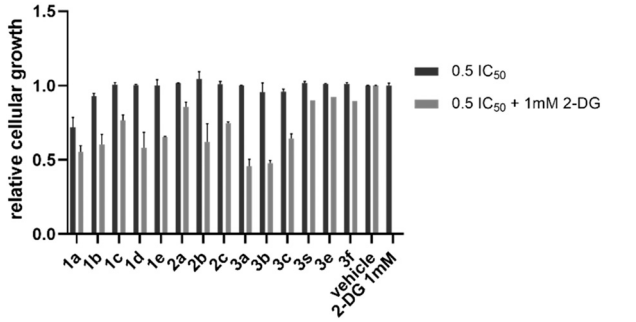

Fig. 5 Relative cellular growth of KP4 cancel cells with 0.5 × IC_{50} of diiminoguanidines and a combination of 0.5 × IC_{50} of diiminoguanidines and 1 mm 2-DG.

prevents its metabolism during glycolysis, effectively blocking the glycolytic pathway. By co-administering 2-DG with our compounds, we can test whether the inhibition of glycolysis unmasks a dependence on mitochondrial respiration—a dependence that would become fatal in the presence of mitochondrial impairment. To this end, we treated KP4 pancreatic cancer cells with a non-toxic concentration of 2-DG (1 mM) in combination with each diiminoguanidine at 0.5 × IC_{50} (Fig. 5). A simple 0.5 × IC_{50} treatment served as the baseline for partial growth inhibition. If the addition of 2-DG had no further effect, this would suggest the mitochondrial function remains intact, and cells are not compensating *via* glycolysis. In contrast, a further reduction in cellular proliferation upon co-treatment would indicate that our compounds impair mitochondrial function and that cells, unable to compensate *via* glycolysis, undergo energy crisis-induced death.

The results were unambiguous: all diiminoguanidines tested exhibited enhanced antiproliferative activity when combined with 2-DG, strongly supporting their inhibitory effect on the mitochondrial respiratory chain. Notably, compound **3b**, already identified as the most potent and selective molecule in the series, produced a ~50% further reduction in cellular viability when used in combination with 2-DG, compared to treatment with **3b** alone. This synergistic effect underscores a robust mitochondrial mechanism of action, reinforcing our earlier microscopy-based conclusions.

Together, these findings provide compelling evidence that diiminoguanidines, particularly compound **3b**, disrupt mitochondrial energy metabolism, and that this disruption is critical to their antiproliferative efficacy. These results also suggest the potential of using glycolytic inhibition as a co-therapeutic strategy to potentiate the effects of mitochondria-targeting agents in pancreatic cancer.

Conclusions

In this study, we successfully synthesized a series of 14 amphiphilic symmetric diiminoguanidinium hydrochloride salts through straightforward, green condensation reactions between *N*,*N*′-diaminoguanidine hydrochloride and a diverse set of aldehydes. By systematically varying the side chains—aromatic, polycyclic aromatic, and heteroaromatic—we modulated both the amphiphilicity and biological activity of the resulting compounds. Biological evaluation on pancreatic cancer cell lines revealed potent antiproliferative activity, with most compounds exhibiting IC_{50} values below 100 μM. Among them, compound **3b**, bearing imidazole side chains, emerged as the lead candidate, with submicromolar IC_{50} values and an excellent selectivity index exceeding 600 when compared to healthy pancreatic and lung fibroblast cell lines. This high efficacy–selectivity profile positions **3b** as a strong candidate for *in vivo* validation.

We identified molecular amphiphilicity (log *P*) as a key determinant of activity: compounds with clog *P* between 0.5 and 4 showed significantly improved potency, suggesting optimal membrane permeability is essential for mitochondrial access. Confocal microscopy confirmed that diiminoguanidines rapidly accumulate in mitochondria, where they persist for at least 24 h—indicating prolonged mitochondrial engagement. Furthermore, combination assays with 2-deoxyglucose provided mechanistic evidence that the mitochondrial respiratory chain is a critical functional target, particularly for compound **3b**.

Taken together, this work introduces a new class of synthetically accessible, mitochondria-targeting anticancer agents with a favorable pharmacological profile for pancreatic cancer. The modular synthesis and tunable side chains offer a promising platform for future optimization toward enhanced selectivity, potency, and translational potential.

Materials and methods

General information

All chemicals were purchased from Sigma Aldrich, Oakwood Chemicals, and Combi-Blocks at their highest purity and were used without further purification. NMR spectra were recorded on AVANCE II 400, Bruker AVANCE NEO 400, Bruker AVANCE 500, and Bruker AVANCE 700 spectrometers. High-resolution mass spectra (HRMS) and LCMS purity analysis were performed on Agilent TOF instruments by the regional mass spectrometry center (University of Montreal).

Synthesis and characterization of compounds

General method for the synthesis of compounds 1a–1e and 2a–2c. To a stirring solution of *N*,*N*′-diaminoguanidine hydrochloride (1 eq.) in methanol (10 mL), aldehyde (2 eq.) was added and the solution was stirred at 80 °C for 6 h. The reaction mixture was then cooled down and concentrated *in vacuo*. *N*,*N*′-Diiminoguanidines hydrochloride salts were obtained from trituration in acetone to obtain the pure product (yield: 18–93%).

*Synthesis of N,N′-di(phenylmethanimino)guanidine hydrochloride (**1a**).* Following the general procedure, *N*,*N*′-diaminoguanidine hydrochloride (1 eq.) and benzaldehyde (2 eq.) yielded compound **1a** as a white powder with a 53%

yield. ^{1}H NMR (400 MHz, DMSO-d_6) δ 12.32 (s, 2H), 8.54 (s, 2H), 8.46 (s, 2H), 7.99–7.90 (m, 4H), 7.55–7.46 (m, 6H). ^{13}C NMR (101 MHz, DMSO-d_6) δ 153.3, 149.3, 133.7, 131.2, 129.2, 128.3. HRMS: m/z [M + H]$^+$ calculated for $C_{15}H_{16}N_5$, 266.1400; found 266.1396.

*Synthesis of N,N′-di(4-fluorophenylmethanimino)guanidine hydrochloride (**1b**).* Following the general procedure, *N*,*N*′-diaminoguanidine hydrochloride (1 eq.) and 4-fluorobenzaldehyde (2 eq.) yielded compound **1b** as a white powder with a 61% yield. ^{1}H NMR (400 MHz, DMSO-d_6) δ 12.36 (s, 2H), 8.57 (s, 2H), 8.45 (s, 2H), 8.04 (dd, J = 8.7, 5.7 Hz, 4H), 7.35 (t, J = 8.8 Hz, 4H). ^{13}C NMR (101 MHz, DMSO-d_6) δ 165.2, 162.7, 153.3, 130.7, 130.6, 130.4, 130.4, 116.4, 116.1. HRMS: m/z [M + H]$^+$ calculated for $C_{15}H_{14}N_5F_2$, 302.1212; found 302.1212.

*Synthesis of N,N′-di(4-chlorophenylmethanimino)guanidine hydrochloride (**1c**).* Following the general procedure, *N*,*N*′-diaminoguanidine hydrochloride (1 eq.) and 4-chlorobenzaldehyde (2 eq.) yielded compound **1c** as a white powder with a 76% yield. ^{1}H NMR (400 MHz, DMSO-d_6) δ 12.43 (s, 2H), 8.62 (s, 2H), 8.45 (s, 2H), 8.00 (d, J = 8.6 Hz, 4H), 7.57 (d, J = 8.5 Hz, 4H). ^{13}C NMR (101 MHz, DMSO-d_6) δ 153.3, 148.1, 135.7, 132.7, 130.0, 129.3. HRMS: m/z [M + H]$^+$ calculated for $C_{15}H_{14}N_5Cl_2$, 334.0621; found 334.0628.

*Synthesis of N,N′-di((3,5-dimethyl)phenylmethanimino) guanidine hydrochloride (**1d**).* Following the general procedure, *N*,*N*′-diaminoguanidine hydrochloride (1 eq.) and 3,5-dimethylbenzaldehyde (2 eq.) yielded compound **1d** as a white powder with a 93% yield. ^{1}H NMR (400 MHz, DMSO-d_6) δ 12.30 (s, 2H), 8.49 (s, 2H), 8.39 (s, 2H), 7.55 (s, 4H), 7.13 (s, 2H), 2.34 (s, 12H). ^{13}C NMR (101 MHz, DMSO-d_6) δ 153.1, 149.5, 138.3, 133.6, 132.7, 126.0, 21.2. HRMS: m/z [M + H]$^+$ calculated for $C_{19}H_{24}N_5$, 322.2026; found 322.2031.

*Synthesis of N,N′-di((3,5-bis(trifluoromethyl)) phenylmethanimino)guanidine hydrochloride (**1e**).* Following the general procedure, *N*,*N*′-diaminoguanidine hydrochloride (1 eq.) and 3,5-bis(trifluoromethyl)benzaldehyde (2 eq.) yielded compound **1e** as a white powder with a 93% yield. ^{1}H NMR (700 MHz, DMSO-d_6) δ 12.64 (s, 2H), 8.90 (s, 2H), 8.70 (s, 4H), 8.58 (s, 2H), 8.21 (s, 2H). ^{13}C NMR (176 MHz, DMSO-d_6) δ 154.0, 146.6, 136.7, 131.6, 131.4, 131.2, 131.0, 128.8, 126.0, 124.5, 123.9, 122.9, 121.4. HRMS: m/z [M + H]$^+$ calculated for $C_{19}H_{12}F_{12}N_5$, 538.0896; found 538.0903.

*Synthesis of N,N′-di(2-naphtylmethanimino)guanidine hydrochloride (**2a**).* Following the general procedure, *N*,*N*′-diaminoguanidine hydrochloride (1 eq.) and 2-naphtaldehyde (2 eq.) yielded compound **2a** as a white powder with a 78% yield. ^{1}H NMR (400 MHz, DMSO-d_6) δ 12.49 (s, 2H), 8.65 (s, 4H), 8.33 (dd, J = 13.6, 4.9 Hz, 4H), 8.10–7.92 (m, 6H), 7.61 (p, J = 5.4 Hz, 4H). ^{13}C NMR (101 MHz, DMSO-d_6) δ 153.2, 149.5, 134.5, 133.1, 131.5, 130.3, 128.9, 128.8, 128.3, 127.9, 127.3, 123.7. HRMS: m/z [M + H]$^+$ calculated for $C_{23}H_{20}N_5$, 366.1713; found 366.1722.

*Synthesis of N,N′-di(phenantrylmethanimino)guanidine hydrochloride (**2b**).* Following the general procedure, *N*,*N*′-diaminoguanidine hydrochloride (1 eq.) and phenantrene-9-carboxaldehyde (2 eq.) yielded compound **2b** as an off-white powder with a 18% yield. ^{1}H NMR (400 MHz, DMSO-d_6) δ 12.51 (s, 2H), 9.45 (s, 2H), 9.05–8.94 (m, 2H), 8.92 (d, J = 8.1 Hz, 2H), 8.75 (s, 2H), 8.72 (s, 2H), 8.59 (dd, J = 6.4 Hz, 3.2 Hz, 2H), 8.16 (d, J = 6.9 Hz, 2H), 7.80 (dddd, J = 15.8 Hz, 14.7 Hz, 6.2 Hz, 1.6 Hz, 8H). ^{13}C NMR (101 MHz, DMSO-d_6) δ 153.0, 131.2, 131.0, 130.5, 129.9, 129.4, 128.6, 128.1, 127.9, 127.7, 124.5, 124.2, 123.5. HRMS: m/z [M + H]$^+$ calculated for $C_{31}H_{24}N_5$, 466.2026; found 466.2026.

*Synthesis of N,N′-di(pyrenylmethanimino)guanidine hydrochloride (**2c**).* Following the general procedure, *N*,*N*′-diaminoguanidine hydrochloride (1 eq.) and pyrene-1-carbaldehyde (2 eq.) yielded compound **2c** as a green powder with a 52% yield. ^{1}H NMR (400 MHz, DMSO-d_6) δ 12.60 (s, 2H), 9.79 (s, 2H), 9.07 (d, J = 8.2 Hz, 2H), 8.80 (s, 2H), 8.63 (d, J = 9.5 Hz, 2H), 8.50–8.34 (m, 8H), 8.30 (q, J = 9.0 Hz, 4H), 8.15 (t, J = 7.6 Hz, 2H). ^{13}C NMR (101 MHz, DMSO-d_6) δ 132.9, 131.2, 130.5, 129.7, 129.4, 129.2, 127.8, 127.1, 126.7, 126.4, 126.4, 125.6, 124.4, 124.2, 122.1. HRMS: m/z [M + H]$^+$ calculated for $C_{35}H_{24}N_5$, 514.2026; found 514.2021.

General method for the synthesis of compounds 3a–3f. To a stirring solution of *N*,*N*′-diaminoguanidine hydrochloride (1 eq.) in methanol (10 mL), aldehyde (2 eq.) was added and the solution was stirred at room temperature for 24 h. The reaction mixture was then cooled down and concentrated *in vacuo*. *N*,*N*′-Diiminoguanidines hydrochloride salts were obtained from trituration in dichloromethane to obtain the pure product (yield: 15–71%).

*Synthesis of N,N′-di(thiophenylmethanimino)guanidine hydrochloride (**3a**).* Following the general procedure, *N*,*N*′-diaminoguanidine hydrochloride (1 eq.) and 2-thiophenecarboxaldehyde (2 eq.) yielded compound **3a** as an orange powder with a 34% yield. ^{1}H NMR (500 MHz, DMSO-d_6) δ 12.29 (s, 2H), 8.65 (s, 2H), 8.24 (s, 2H), 7.79 (d, J = 5.0 Hz, 2H), 7.62 (dd, J = 3.6, 0.9 Hz, 2H), 7.19 (dd, J = 5.0, 3.6 Hz, 2H), 3.40 (s, 2H). ^{13}C NMR (126 MHz, DMSO-d_6) δ 152.6, 144.5, 137.8, 132.7, 130.8, 128.4. HRMS: m/z [M + H]$^+$ calculated for $C_{11}H_{12}N_5S_2$, 278.0529; found 278.0530.

*Synthesis of N,N′-di(imidazolemethan-2-imino)guanidine hydrochloride (**3b**).* Following the general procedure, *N*,*N*′-diaminoguanidine hydrochloride (1 eq.) and imidazole-2-carboxaldehyde (2 eq.) yielded compound **3b** as a beige powder with a 15% yield. ^{1}H NMR (400 MHz, DMSO-d_6) δ 12.53 (s, 4H), 7.97 (s, 2H), 7.38 (s, 2H), 7.26 (s, 4H). ^{13}C NMR (176 MHz, DMSO-d_6) δ 144.3, 141.8, 133.8, 123.8. HRMS: m/z [M + H]$^+$ calculated for $C_9H_{12}N_9$, 246.1210; found 246.1220.

*Synthesis of N,N′-di(pyridinylmethan-2-imino)guanidine hydrochloride (**3c**).* Following the general procedure, *N*,*N*′-diaminoguanidine hydrochloride (1 eq.) and pyridine-2-carboxaldehyde (2 eq.) yielded compound **3c** as a yellow powder with a 36% yield. ^{1}H NMR (400 MHz, DMSO-d_6) δ 12.73 (s, 2H), 8.75 (s, 2H), 8.67–8.66 (d, J = 4 Hz, 2H), 8.52 (s, 2H), 8.48–8.40 (d, J = 8 Hz, 2H), 8.00–7.96 (t, J = 7.2 Hz, 2H), 7.52–7.49 (t, J = 4.8 Hz, 2H). ^{13}C NMR (126 MHz, DMSO-d_6) δ 152.5, 149.7, 137.8, 125.5, 121.9. HRMS: m/z [M + H]$^+$ calculated for $C_{13}H_{14}N_7$, 268.1305; found 268.1315.

*Synthesis of N,N′-di(pyrole-2-methanimino)guanidine hydrochloride (**3d**).* Following the general procedure, *N*,*N*′-diaminoguanidine hydrochloride (1 eq.) and pyrole-2-carboxaldehyde (2 eq.) yielded compound **3d** as a khaki powder with a 71% yield. ^{1}H NMR (400 MHz, DMSO-d_6) δ 12.69 (s, 2H), 11.80 (s, 2H), 8.24 (s, 4H), 7.05 (s, 2H), 6.52 (s, 2H), 6.15–6.14 (m, 2H). ^{13}C NMR (126 MHz, DMSO-d_6) δ 152.8, 139.7, 127.5, 123.0, 114.2, 109.8. HRMS: m/z $[M + H]^+$ calculated for $C_{11}H_{14}N_7$, 244.1305; found 244.1315.

*Synthesis of N,N′-di(indole-5-methanimino)guanidine hydrochloride (**3e**).* Following the general procedure, *N*,*N*′-diaminoguanidine hydrochloride (1 eq.) and indole-5-carboxaldehyde (2 eq.) yielded compound **3e** as a pink powder with a 68% yield. ^{1}H NMR (400 MHz, DMSO-d_6) δ 12.04 (s, 2H), 11.49 (s, 2H), 8.48 (s, 2H), 8.32 (s, 2H), 8.03 (s, 2H), 7.82–7.80 (d, J = 8.5 Hz, 2H), 7.50 (s, 2H), 7.48 (s, 2H), 7.44 (s, 2H), 6.54 (s, 2H). ^{13}C NMR (126 MHz, DMSO-d_6) δ 131.0, 127.1, 122.3, 120.7, 112.6, 102.5. HRMS: m/z $[M + H]^+$ calculated for $C_{19}H_{18}N_7$, 344.1618; found 344.1629.

*Synthesis of N,N′-di(pyrimidine-5-methanimino)guanidine hydrochloride (**3f**).* Following the general procedure, *N*,*N*′-diaminoguanidine hydrochloride (1 eq.) and 5-formylpyrimidine (2 eq.) yielded compound **3f** as a yellow powder with a 53% yield. ^{1}H NMR (400 MHz, DMSO-d_6) δ 12.70 (s, 2H), 9.37 (s, 4H), 9.26 (s, 2H), 8.77 (s, 2H), 8.50 (s, 2H). ^{13}C NMR (126 MHz, DMSO-d_6) δ 159.4, 156.3, 143.6, 128.3. HRMS: m/z $[M + H]^+$ calculated for $C_{11}H_{12}N_9$, 270.121; found 270.1220.

Biological assays

General information. Absorbance measurements for the determination of IC_{50} values were performed using a SpectraMax 190 microplate reader from molecular devices. The obtained data were analyzed with PRISM software by fitting *a* curve with nonlinear regression (log(inhibitor) *vs.* response – variable slope (four parameters)). *hTERT*-HPNE cells (*hTERT*-immortalized epithelial cells) were obtained from Dr. M. Ouellette (University of Nebraska, Medical Center). The pancreatic cells PANC-1 (epithelial morphology cell line isolated from the pancreatic duct of a 56-year-old white male with an epithelioid carcinoma) and KP-4 (human pancreatic ductal carcinoma cell line derived from human ascites) were obtained from ATCC or the Massachusetts General Hospital Center for Molecular Therapeutics (CMT).

Cellular growth assay. KP4, PANC1, IMR90, and *hTERT*-HPNE cells were cultured in DMEM (319-015-CL, Wisent) supplemented with 10% fetal bovine serum (FBS, Wisent) and penicillin/streptomycin/L-glutamine (Wisent) at 37 °C with 5% CO_2. The cells were seeded at a density of 1×10^3 cells per well for KP4 and PANC1, and 4×10^3 for IMR90 and *hTERT*-HPNE in 96-well plates for 24 hours. Following this, treatments with different concentrations of vehicle (4% DMSO) and compounds were carried out for 72 hours. The culture medium was then removed. The cells were washed twice with cold PBS to remove any dead cells. A 1% glutaraldehyde solution was added to the wells for 10 minutes to fix the remaining viable cells. The cells were then washed with PBS, stained with 0.2% violet crystal for 30 minutes at room temperature, washed with water, and dried. The adherent violet crystal was solubilized in 10% acetic acid, and absorbance was measured at a wavelength of 590 nm to calculate cell viability.

UV-vis stability analysis. Solutions of diiminoguanidine hydrochlorides were prepared in PBS buffer with 4% DMSO to mimic the dilution conditions used for the *in vitro* assays. A first UV-vis spectrum was recorded and named "day 0" to be used as a reference for the maximum wavelength of absorption. The solutions were heated at 37 °C for 3 days, and a spectrum was recorded everyday and names "day 1", "day 2" and "day 3".

Fluorescence microscopy. KP4 cancer cells were seeded at a density of 8×10^4 cells per well on microscope slides in 6-well plates overnight. They were then treated with either the vehicle or the studied compounds for the desired treatment times (30 min, 2 h, 4 h, 24 h). The culture medium was replaced, and a solution of MitoTracker® Deep Red FM (100 nM in DMEM) was added. After 30 minutes at 37 °C, the medium was removed. The cells were washed twice with PBS. A 4% paraformaldehyde solution was added to the wells for 10 minutes to fix the cells onto the microscope slides. The cells were then washed three times with a 0.1 M glycine solution in PBS. 8 μL of mounting medium for fluorescence without DAPI was used to mount each slide onto a microscope slide. The slides were sealed, dried, and observed under a microscope. Microscopy images were acquired using the Zeiss Axio-Imager Z2 Microscope. The fluorescence filter sets used were: GFP HE (Zeiss Set 38): BP 470/40x FT 495 BP 525/50 m; Cy5 (Chroma 49009): BP ET640/30x BS TLPXR660 BP ET690/50 m, along with the DIC analyser.

Author contributions

A. R. S. and S. L. for conceptualization of the project. S. L. for investigation and synthesis of the compounds and biological studies. S. L. for the original draft preparation. S. L. and A. R. S. for writing, review and editing. All authors have given approval to the final version of the manuscript.

Conflicts of interest

There are no conflicts to declare.

Data availability

The data supporting this article have been included as part of the supplementary information (SI).

Supplementary information: ^{1}H and ^{13}C NMR spectra, mass spectrometry, purity, biological tests and IC_{50} determination, selectivity indexes on PANC1 cancer cells, excitation and emission spectra of diiminoguanidines,

stability assays, confocal microscopy images. See DOI: https://doi.org/10.1039/d5md00808e.

Acknowledgements

This research was funded by Natural Sciences and Engineering Research Council, grant number RGPIN-2021-03128. We thank G. Ferbeyre from the Département de Biochimie et de Médecine moléculaire, S. Cecioni from the Département de Chimie and the Plateforme de microcopie de l'Université de Montréal for access to their laboratories and instruments. Access to the NMR *via* the Regional Centre for Magnetic Resonance (UdeM – Chemistry) was possible due to funding from the Canada Foundation for Innovation and the Institute Courtois.

Notes and references

1 C. J. Cabasag, J. Ferlay, M. Laversanne, J. Vignat, A. Weber, I. Soerjomataram and F. Bray, *Gut*, 2022, **71**(8), 1686–1687.
2 C. J. Halbrook, C. A. Lyssiotis, M. Pasca di Magliano and A. Maitra, *Cell*, 2023, **186**(8), 1729–1754.
3 L. Rahib, M. R. Wehner, L. M. Matrisian and K. T. Nead, *JAMA Netw. Open*, 2021, **4**(4), e214708–e214708.
4 L. Rahib, B. D. Smith, R. Aizenberg, A. B. Rosenzweig, J. M. Fleshman and L. M. Matrisian, *Cancer Res.*, 2014, **74**(11), 2913–2921.
5 A. P. Klein, *Nat. Rev. Gastroenterol. Hepatol.*, 2021, **18**(7), 493–502.
6 E. E. Montalvo-Javé, N. Nuño-Lámbarri, G. N. López-Sánchez, E. A. Ayala-Moreno, G. Gutierrez-Reyes, J. Beane and T. M. Pawlik, *J. Gastrointest. Surg.*, 2023, **27**(5), 1001–1010.
7 R. Pothuraju, S. Rachagani, W. M. Junker, S. Chaudhary, V. Saraswathi, S. Kaur and S. K. Batra, *J. Exp. Clin. Cancer Res.*, 2018, **37**(1), 319.
8 J. Zheng, M. A. Guinter, A. T. Merchant, M. D. Wirth, J. Zhang, R. Z. Stolzenberg-Solomon and S. E. Steck, *Nutr. Rev.*, 2017, **75**(11), 883–908.
9 T. J. Grant, K. Hua and A. Singh, *Prog. Mol. Biol. Transl. Sci.*, 2016, **144**, 241–275.
10 S. E. Kern, R. H. Hruban, M. Hidalgo and C. J. Yeo, *Cancer Biol. Ther.*, 2002, **1**(6), 607–613.
11 G. Z. Murimwa, J. D. Karalis, J. Meier, M. Nehrubabu, M. Thornton, M. Porembka, S. Wang, H. J. Zeh, A. C. Yopp and P. M. Polanco, *J. Surg. Oncol.*, 2023, **128**(4), 540–548.
12 C. W. Choi, I. K. Choi, J. H. Seo, B. S. Kim, J. S. Kim, C. D. Kim, S. H. Um, J. S. Kim and Y. H. Kim, *Am. J. Clin. Oncol.*, 2000, **23**(4), 425–428.
13 D. B. Longley, D. P. Harkin and P. G. Johnston, *Nat. Rev. Cancer*, 2003, **3**(5), 330–338.
14 W. B. Wang, Y. Yang, Y. P. Zhao, T. P. Zhang, Q. Liao and H. Shu, *World J. Gastroenterol.*, 2014, **20**(42), 15682–15690.
15 N. S. Siddiqui, A. Godara, M. M. Byrne and M. W. Saif, *Expert Opin. Pharmacother.*, 2019, **20**(4), 399–409.
16 D. B. Smith and J. P. Neoptolemos, *Core Evidence*, 2007, **2**(2), 111–119.
17 T. H. Cartwright, A. Cohn, J. A. Varkey, Y.-M. Chen, T. P. Szatrowski, J. V. Cox and J. J. Schulz, *J. Clin. Oncol.*, 2002, **20**(1), 160–164.
18 M. K. Chllamma, N. Cook, N. C. Dhani, K. Giby, A. Dodd, L. Wang, D. W. Hedley, M. J. Moore and J. J. Knox, *Br. J. Cancer*, 2016, **115**(6), 649–654.
19 C. Nitipir, R. Vrabie, A. I. Parosanu, R. Tulin, B. Cretu, A. Cursaru, I. Slavu, A. Miron, V. Calu and M. C. Orlov Slavu, *Cureus*, 2021, **13**(11), e19361.
20 H. L. Kindler, *American Society of Clinical Oncology Educational Book*, 2012, vol. 32, pp. 232–237.
21 D.-C. Chi, F. Brogan, I. Turenne, S. Zelonis, L. Schwartz and M. W. Saif, *Anticancer Res.*, 2012, **32**(9), 4147.
22 H. A. Burris, M. J. Moore, J. Andersen, M. R. Green, M. L. Rothenberg, M. R. Modiano, M. C. Cripps, R. K. Portenoy, A. M. Storniolo, P. Tarassoff, R. Nelson, F. A. Dorr, C. D. Stephens and D. D. V. Hoff, *J. Clin. Oncol.*, 2023, **41**(36), 5482–5492.
23 Y. J. Min, K. R. Joo, N. H. Park, T. K. Yun, Y. W. Nah, C. W. Nam and J. H. Park, *Korean J. Intern. Med.*, 2002, **17**(4), 259–262.
24 W. Plunkett, P. Huang, Y. Z. Xu, V. Heinemann, R. Grunewald and V. Gandhi, *Semin. Oncol.*, 1995, **22**(4), 3–10.
25 B. Hryciuk, B. Szymanowski, A. Romanowska, E. Salt, B. Wasąg, B. Grala, J. Jassem and R. Duchnowska, *Oncol. Lett.*, 2018, **15**(2), 1912–1916.
26 J. S. Armstrong, *Br. J. Pharmacol.*, 2007, **151**(8), 1154–1165.
27 C. Wang and R. J. Youle, *Annu. Rev. Genet.*, 2009, **43**, 95–118.
28 F. Fontanesi, *Mitochondria: Structure and Role in Respiration*, eLS, pp. 1–13.
29 H. Wang, B. Fang, B. Peng, L. Wang, Y. Xue, H. Bai, S. Lu, N. H. Voelcker, L. Li, L. Fu and W. Huang, *Front. Chem.*, 2021, **9**, 683220.
30 F. J. Bock and S. W. G. Tait, *Nat. Rev. Mol. Cell Biol.*, 2020, **21**(2), 85–100.
31 T. T. Nguyen, S. Wei, T. H. Nguyen, Y. Jo, Y. Zhang, W. Park, K. Gariani, C.-M. Oh, H. H. Kim, K.-T. Ha, K. S. Park, R. Park, I.-K. Lee, M. Shong, R. H. Houtkooper and D. Ryu, *Exp. Mol. Med.*, 2023, **55**(8), 1595–1619.
32 D. R. Green and J. C. Reed, *Science*, 1998, **281**(5381), 1309–1312.
33 A. Hébert, M. Parisotto, G. Ferbeyre and A. R. Schmitzer, *Supramol. Chem.*, 2019, **31**(3), 127–139.
34 A. Hébert, M. Parisotto, M.-C. Rowell, A. Doré, A. Fernandez Ruiz, G. Lefrançois, P. Kalegari, G. Ferbeyre and A. R. Schmitzer, *Sci. Rep.*, 2021, **11**(1), 9854.
35 J. Vatté, V. Bourdeau, G. Ferbeyre and A. R. Schmitzer, *Molecules*, 2024, **29**(16), 3773–3786.
36 J. Vatté, V. Bourdeau, G. Ferbeyre and A. R. Schmitzer, *Molecules*, 2024, **29**(22), 5329–5355.
37 B. Juliana de Oliveira Carneiro, F. Tanos Celmar Costa, R. L. Steven and V. José Daniel Figueroa, *Mini-Rev. Med. Chem.*, 2020, **20**(5), 342–368.

